AIP | Applied Physics Letters

A superconducting antenna-coupled hot-spot microbolometer

A. Luukanen and J. P. Pekola

Citation: Applied Physics Letters **82**, 3970 (2003); doi: 10.1063/1.1579562
View online: http://dx.doi.org/10.1063/1.1579562
View Table of Contents: http://scitation.aip.org/content/aip/journal/apl/82/22?ver=pdfcov
Published by the AIP Publishing

A superconducting antenna-coupled hot-spot microbolometer

A. Luukanen[a)]
Department of Physics, University of Jyväskylä, P.O. Box 35(Y5), FIN-40014, Finland and Metorex International Oy, P.O. Box 85, FIN-02631, Espoo, Finland

J. P. Pekola
Low Temperature Laboratory, Helsinki University of Technology, P.O. Box 2200, FIN-02015 HUT, Finland

(Received 24 January 2003; accepted 31 March 2003)

We report the electrical properties of an antenna-coupled niobium vacuum-bridge bolometer, operated at a temperature of 4.2 K, in which the thermal isolation is maximized by the vacuum gap between the bridge and the underlying silicon substrate. The device is voltage-biased, which results in a formation of a normal state region in the middle of the bridge. The device shows a current responsivity of -1430 A/W and an amplifier limited electrical noise equivalent power of 1.4×10^{-14} W/$\sqrt{\text{Hz}}$. © *2003 American Institute of Physics.* [DOI: 10.1063/1.1579562]

Antenna coupling extends the detectable range of wavelengths of bolometers to millimeter waves and beyond.[1–4] Antenna-coupled microbolometers consist of a lithographic antenna, coupled electrically to a thermally sensitive element. Incident electromagnetic radiation induces time-varying current in the antenna, which is dissipated in an impedance-matched bolometer element acting as the antenna termination. Measurements have shown that nearly perfect optical coupling is possible up to 30 THz.[5] One of the main benefits of this technology is that the sensitivity is not limited by thermal time constant requirements, unlike the case of the state-of-the-art infrared micromachined microbolometers,[6] as well as in several other bolometer experiments. The noise equivalent power (NEP) is $(4k_BT^2C/\tau_0)^{1/2}$ for a phonon-noise-limited bolometer with a heat capacity C, a thermal time constant $\tau_0=C/G$, and G the thermal conductance between the bolometer and the heat sink. In antenna-coupled devices, the thermal sensing element can be made much smaller than the detected wavelength, resulting in a much smaller heat capacity, thus allowing for smaller G and better NEP. Previously, antenna-coupled high-T_c vacuum-bridge microbolometers showed excellent performance with a NEP$=9\times10^{-12}$ W/$\sqrt{\text{Hz}}$ at a bath temperature of 87.4 K.[7] However, the fabrication of such vacuum bridges has proven to be difficult. Additionally, high-T_c films usually require a buffer layer, such as yttrium stabilized zirconia, and they often suffer from high levels of $1/f$ noise, thus requiring the use of an optical chopper.

If operated at or close to the temperature of liquid helium, conventional superconductors such as Nb can be used. Besides the relatively simple processing, the thermal fluctuation and Johnson noise of the bolometer are significantly lower at 4.2 K, as compared to 77 K. A convenient way of biasing superconducting transition-edge sensors is by constant voltage, as is done with x-ray microcalorimeters.[8] This results in a formation of a normal state region, which in the vacuum-bridge device is located in the center portion of the bridge.[9,10] To model the performance of the vacuum bridge, we first assume that the electron and phonon populations are at equilibrium; that is, $T_e=T_p$. We also consider a steady-state treatment, since we estimate $\tau_0\sim1\ \mu$s, which is much faster than any typical signal to be detected. The heat flow in the normal region of the bridge is in the steady state given by $-\kappa d^2T/dx^2=V^2/(\rho l_n)^2\rho+P_{\text{opt}}/(wtl_n)$, with $|x|<l_n/2$, while in the superconducting part, $-\kappa d^2T/dx^2=P_{\text{opt}}/(wtl)$, with $|x|>l_n/2$. These equations include the assumption that part of the bridge is in the normal state and that the thermal conductivity κ is same and constant in both regions. We base this rather bold assumption on the fact that at this range of temperatures, the contribution of the lattice to the thermal conductivity is significant, and can even *increase* below T_c in disordered metals due to the reduced electron–phonon scattering as the number of quasiparticles decreases, so that the changes in the sum of the lattice and the electronic contributions remain relatively small.[11] The bridge (length l, width w, thickness t) is biased with voltage V, and has a normal state resistivity ρ. The length of the normal state part of the wire is given by l_n. Dissipation of both the bias power P_b and the optical power $P_{\text{opt}}(\ll P_b)$ takes place in the normal part of the wire, whereas the superconducting region of the bridge is assumed to dissipate only the rf. It should be noted that frequencies slightly below the gap frequency of Nb ($f=3.52k_BT_c/h=500$ GHz with $T_c=6.8$ K) are absorbed in the superconducting region as there is a large temperature gradient present in the bridge.

We use boundary conditions $T(0)=T(l)=T_0$, and $dT(l_n/2)/dx|_S=dT(l_n/2)/dx|_N$ at the superconducting–normal interfaces. Additionally, we require the maximum of the temperature to occur at the middle of the normal state part; that is, that $dT/dx|_{l/2}=0$.

In the limit of small optical power, $P_{\text{opt}}\to0$, the solution for the $I(V)$ reduces to

$$I(V)_0=\frac{4\kappa(T_c-T_0)wt}{Vl}+\frac{Vwt}{\rho l}. \tag{1}$$

The first term on the right side of Eq. (1) is due to the electrothermal feedback, while the second term on the right describes the ohmic behavior of the bridge. When V

a)Present address: VTT Information Technology, Microsensing, P.O. Box 1207, FIN-02044 VTT, Finland; electronic mail: arttu.luukanen@vtt.fi

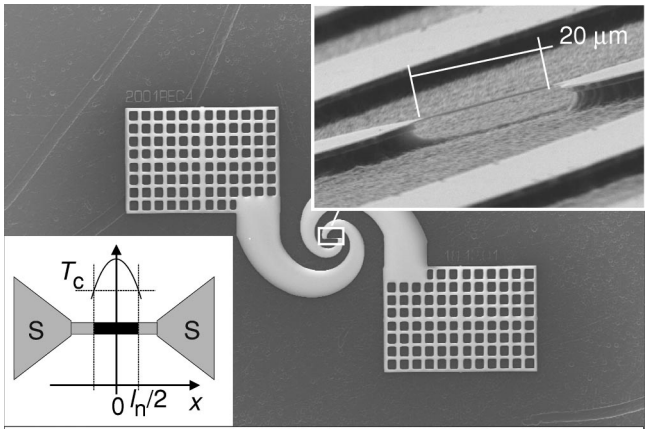

FIG. 1. A scanning electron micrograph of the antenna-coupled Nb bridge bolometer. The inset at upper right shows a detailed image of the feed region taken at a steep angle to show the separation between the bridge and the substrate. The diagram at lower left shows the model used in the theoretical treatment with S indicating the superconducting regions, and the shaded area in the middle of the bridge marking the normal region extending from $-l_n/2$ to $l_n/2$.

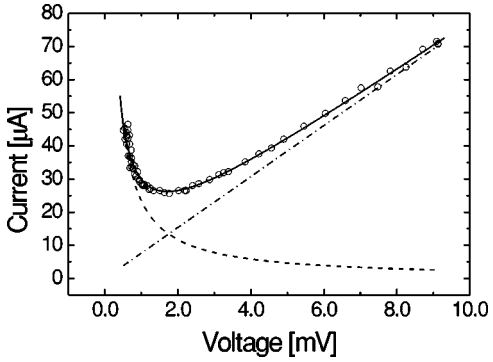

FIG. 2. The $I-V$ curve of the parallel connection of the Nb vacuum bridge and the shunt resistor (circles). The linear part towards higher voltage values corresponds to the ohmic behavior of the bridge in its normal state. The fit with the theory is given by the solid line with $\kappa=0.54$ W/Km. As a reference, the asymptote corresponding to the ohmic behavior ($\propto V$) is marked with a dash-dotted line. At voltages below about 1.8 mV, the ends of the bridge turn superconducting, resulting in negative differential resistance and dissipation that are independent of the bias voltage. The dashed line represents the electrothermal term which is proportional to $1/V$. The noise present in the experimental data arises from the bias source.

is small, the bias dissipation is constant and equal to $4\kappa(T_c-T_0)wt/l$. Saturation occurs when optical power approaches the bias power.

The 20-μm$\times$1-μm$\times$100-nm Nb vacuum bridge is fabricated on a nitridized high-resistivity Si wafer. The nominal thickness of the nitride was 1 μm. For convenience, we use electron-beam lithography to pattern the structures, although optical lithography could be used as well. The antenna and the bolometer bridge are patterned using electron-beam lithography on electron resist with a thickness of 650 nm. The antenna is a logarithmic spiral antenna with a nominal band from 455 GHz to 2 THz determined by the outer and inner radii of the spiral, respectively, and a real input impedance of 75 Ω on Si ($\epsilon_r=11.7$). Following the patterning, a 100-nm-thick Nb layer is evaporated at a rate of 3 Å/s. After lift-off, the sample is dry etched with a mixture of CF_4 and O_2 gases. This dry etching step removes the Si_3N_4 from the sample. The etch is performed at a relatively high pressure of 50 mTorr, which results in isotropic etch of the nitride, removing it also underneath the narrow Nb bridge. By prolonging the etching step it is also possible to etch the bulk Si, exposed after the Si_3N_4 has been removed. The resulting bridge is separated by a $\sim$2-μm vacuum gap from the underlying substrate (see Fig. 1). Some underetch ($\sim$1 μm laterally) of the antenna also takes place, but we believe that this has a negligible effect on the antenna properties. As the devices were intended for electrical measurements only, the antenna does not incorporate thicker normal metal layer required to prevent losses in the relatively thin Nb film.

The critical temperature and resistivity of the Nb was measured in an independent four-wire measurement against a coulomb blockade primary thermometer (CBT),[12] yielding $T_c=6.8$ K and $\rho=56\mu\Omega$ cm. After this, the devices were characterized by measuring their current–voltage characteristics with a superconducting quantum interference device (SQUID) current preamplifier.[13] The sample, together with the SQUID encased in a superconducting Nb shield, were mounted to a vacuum can immersed in liquid helium. A floating bias circuit consisted of a tunable 18-V battery, connected in series with a 1.2-kΩ current limiting resistor at room temperature. The voltage bias for the bridge was provided by a 1.2-Ω shunt resistor connected in parallel with the bridge (see Fig. 2).

Using Eq. (1), a fit was made to the $I-V$ curve with κ as a fit parameter. All the other parameters were fixed. For the thermal conductivity we obtained $\kappa=0.54$ W/Km, which is surprisingly close to the value predicted by the Wiedemann–Franz law, $L_0T_c/\rho=0.29$ W/Km with $L_0=2.45\times10^{-8}$ V^2/K^2, and to that reported for NbTi (0.26 W/Km).[14] We attribute this to the contribution of the phonons to the thermal conductivity below T_c.

For any resistive bolometer, the electrical responsivity can be calculated from the $I-V$ curve using the differential ($Z=dV/dI$) and bias point resistance ($R=V/I$).[15] The parameter describing the negative electrothermal feedback (ETF) in the bolometer is the loop gain, given by $\mathcal{L}=\beta(Z-R)/(Z+R)$, and can be calculated from Eq. (1), yielding $\mathcal{L}=4\beta\kappa\rho(T_c-T_0)/V^2$. Here, $\beta=(R-R_s)/(R+R_s)$ describes the influence of the voltage source impedance on the ETF. Again, we have omitted the frequency dependence of $\mathcal{L}$ as we assume that the device response is much faster than any typical signal. A general treatment of a voltage biased bolometer yields a current responsivity $S_I\equiv dI/dP\approx-V^{-1}\mathcal{L}/(\mathcal{L}+1)$, which approaches a value $-1/V$ when $\mathcal{L}$ is large. Figure 3 shows the current responsivity determined from the $I-V$ curve.

Noise measurements were performed by biasing the bridge at different points on the $I-V$ curve, and measuring the rms noise between 750 Hz and 25 kHz. The noise consists of uncorrelated contributions from the fluctuations of heat between the bridge and the heat sink (phonon noise), Johnson noise of the resistive part, and noise from the SQUID. The phonon noise current is given by $i_p=\sqrt{\gamma 4k_BT_c^2G}|S_I|$, where $\gamma=0.67$ describes the effect of the temperature gradient in the bridge.[16] The Johnson current noise is not amplified by the electrothermal gain, and is given at the sensor output by $i_J=\sqrt{4k_BT_c/R}(1+\beta)/[2(1+\mathcal{L})]$. The current noise of the SQUID was measured

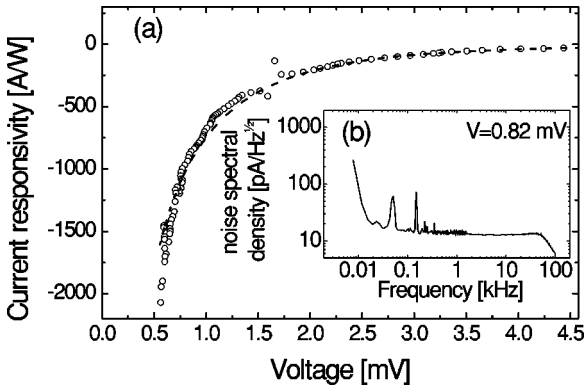

FIG. 3. (a) The electrical responsivity of the bridge derived from the $I-V$ curve (circles). A 30-point adjacent averaging method was used to smooth the experimental data. The dashed line is the responsivity calculated using the fit to the $I-V$ characteristics. (b) Noise spectrum of the detector at $V=0.82$ mV. The cutoff at ~ 50 kHz corresponds to the bandwidth of the SQUID flux-locked loop electronics. The low-frequency noise seen below 10 Hz is attributed to the SQUID since it was not effected by the voltage.

separately yielding $i_{sq}=12$ pA/$\sqrt{\text{Hz}}$. The total NEP of the detector is given by $\text{NEP}_{tot}^2=(i_p^2+i_J^2+i_{sq}^2)/|S_I|^2$.

The results of the noise measurement are shown in Fig. 4 with a comparison to the theoretical prediction described earlier. The minimum NEP is reached at $V=0.82$ mV where $\text{NEP}=1.4\times10^{-14}$ W/$\sqrt{\text{Hz}}$, which is almost an order of magnitude improvement over existing 4.2-K bolometers. Furthermore, improvement of the read-out noise would improve the NEP further down to the detector limited NEP of 2.6×10^{-15} W/$\sqrt{\text{Hz}}$. Also noteworthy is the excellent dynamic range of the device: The bias dissipation is 26 nW, yielding dynamic range of 55 dB at a 30-Hz information bandwidth. The increase in the NEP seen below 0.82 mV arises from oscillations of the electrical circuit. The intrinsic time constant is $\tau_0\approx0.9$ μs based on the heat capacity for

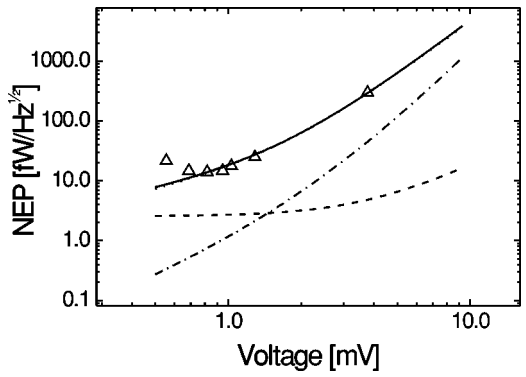

FIG. 4. The electrical NEP of the bolometer. The measured NEP is marked by triangles, and the solid line corresponds to the modeled data, which includes contributions from thermal fluctuation noise (dashed line), Johnson noise (dash-dotted line), and SQUID noise (dots). The NEP is limited by the noise of the SQUID until $V=0.82$ mV. The increase in the noise below this point is due to oscillations of the bias circuit as the effective time constant τ_{eff} becomes comparable to the electrical time constant τ_{ele}.

the bridge in the normal state, and the measured value for G, whereas the time constant of the bias circuit is $\tau_{ele}=L/R$ where $L\approx2$ μH is the combined inductance of the SQUID input coil and parasitic inductance from wiring. At $V=0.82$ mV, $R=28$ Ω, $\mathcal{L}=4.5$, and thus $\tau_{eff}/\tau_{ele}=\tau_0(1+\mathcal{L})^{-1}\tau_{ele}^{-1}\approx2$, while the stability criterion requires this ratio to be more than 5.8.[17]

Some coupling mismatch is present due to the slightly larger resistance of the bridge (130 Ω versus the 75 Ω of the antenna), and to the inductance of the bridge. Taking in account the resistance and the 10-pH self inductance of the bridge, we estimate the impedance mismatch between the antenna and the bridge will reflect less than 20% of the optical power at all bias points if operated around 500 GHz.

In summary, we have modeled, fabricated, and measured the electrical properties of a superconducting bolometer with an electrical NEP better by almost an order of magnitude compared to the current state-of-the-art bolometers operated at 4.2 K. The simple fabrication process allows the construction of large imaging arrays, while improving the noise matching with the SQUID would allow for a further significant improvement of NEP. The detector is compatible with SQUID multiplexing methods,[18] which make it an attractive choice for large imaging millimeter wave arrays.

The authors would like to thank K. Hansen, H. Sipilä, and T. Suppula for discussions. This work has been funded by the Academy of Finland and the Finnish technology agency TEKES within the framework of National ANTARES space research programs High Energy Astrophysics and Space Astronomy (HESA) consortium.

[1] T.-L. Hwang, S. Schwarz, and D. Rutledge, Appl. Phys. Lett. **34**, 773 (1979).
[2] D. P. Neikirk and D. B. Rutledge, Appl. Phys. Lett. **44**, 153 (1984).
[3] M. E. MacDonald and E. N. Grossman, IEEE Trans. Microwave Theory Tech. **43**, 893 (1995).
[4] A. Luukanen and V.-P. Viitanen, Proc. SPIE **3378**, 34 (1998).
[5] E. N. Grossman, J. E. Sauvageau, and D. G. McDonald, Appl. Phys. Lett. **59**, 3225 (1991).
[6] R. Wood, *Monolithic Silicon Microbolometer Arrays, Semiconductors and Semimetals* Vol. 47 (Academic, New York, 1997), Chap. 3, pp. 43-122.
[7] J. Rice, E. Grossman, and D. Rudman, Appl. Phys. Lett. **65**, 773 (1994).
[8] K. D. Irwin, Appl. Phys. Lett. **66**, 1998 (1995).
[9] D. W. Floet, E. Miedema, and T. Klapwijk, Appl. Phys. Lett. **74**, 433 (1999).
[10] H. F. Merkel, P. Khosropanah, S. Cherednichenko, K. Yngvesson, A. Adam, and E. L. Kollberg, IEEE Trans. Appl. Supercond. **11**, 179 (2001).
[11] S. Wasim and N. Zebouni, Phys. Rev. **187**, 539 (1969).
[12] Nanoway Oy, CBT primary thermometer, sensor CBT10, monitor model 400R.
[13] Conductus iMAG LTS SQUID system.
[14] F. Pobell, *Matter and Methods at Low Temperatures*, 2nd ed. (Springer, Berlin, 1996).
[15] R. C. Jones, J. Opt. Soc. Am. **43**, 1 (1953).
[16] J. C. Mather, Appl. Opt. **21**, 1125 (1982).
[17] K. D. Irwin, G. C. Hilton, D. A. Wollman, and J. M. Martinis, J. Appl. Phys. **83**, 3978 (1998).
[18] M. Kiviranta, H. Seppä, J. van der Kuur, and P. Korte, AIP Conf. Proc. **605**, 295 (2002).